Vertical heat transfer in the Arctic Ocean: The role of double-diffusive mixing

Anders Sirevaag[1,2] and Ilker Fer[1,2]

Received 23 January 2012; revised 25 April 2012; accepted 25 May 2012; published 13 July 2012.

[1] Microstructure profiles collected in the central Amundsen Basin are analyzed in order to quantify the role of double-diffusive mixing for vertical heat transfer from the Atlantic layer. In the profiles, a persistent, but laterally incoherent thermohaline staircase structure is identified in the 200–260 m depth range. The staircase contains homogeneous layers with average height of 1.3 m and thin, high-gradient interfaces with average temperature and salinity jumps of about 0.065°C and 0.015, respectively. When inferred from a commonly used diffusive convection parameterization, the average vertical heat flux within the staircase is 0.6 W m^{-2}. This is one order of magnitude larger than the molecular diffusion alone and of the same order as the overall heat loss from the Atlantic layer in the deep basins of the Arctic Ocean. The parameterization is evaluated using observed turbulent heat fluxes and is found to overestimate diffusive convective fluxes with up to an order of magnitude, especially for weak thermal forcing (small temperature jumps in staircase). Staircases coexist with thermohaline intrusions in the vertical temperature and salinity profiles. Lomonosov Ridge is identified as a potential region for formation of intrusions. It is found that salt fingering is the dominant process during intrusion growth whereas diffusive convection is the dominant process in maintaining the intrusions at steady state in the deep basins.

Citation: Sirevaag, A., and I. Fer (2012), Vertical heat transfer in the Arctic Ocean: The role of double-diffusive mixing, *J. Geophys. Res.*, *117*, C07010, doi:10.1029/2012JC007910.

1. Introduction

[2] The inflow of warm Atlantic Water into the Arctic Ocean through the Fram Strait alone would be enough to melt the Arctic sea ice within four years [*Turner*, 2010]. The vertical mixing in the Arctic water column, however, is weak [*Fer*, 2009; *Rainville and Winsor*, 2008] and the major part of the heat transfer is hypothesized to occur along boundaries [*Padman*, 1995], where the stratification of the upper ocean is weaker, and the core of the inflow is warmer and turbulent [*Lenn et al.*, 2009; *Perkin and Lewis*, 1984; *Sirevaag and Fer*, 2009]. *Aagaard and Greisman* [1975] estimated the net heat supply into the Arctic in Fram Strait to be 55 TW, of which 14 TW is estimated to be lost to ice melting and atmosphere immediately north of Svalbard [*Rudels et al.*, 2008]. Of the remaining 41 TW entering the Arctic Ocean about 12 TW is estimated to be lost from the Atlantic layer in 'hot spots' of mixing near boundaries and over rough topography assumed to cover 30% of the Arctic Ocean surface of 10^{13} m^2 [*Fer et al.*, 2010]. The average heat loss from the Atlantic layer in the Arctic basins away from topography is then around 4 W m^{-2}. The relatively quiescent interior water column and the hydrography favorable for double diffusion convection suggest that vertical heat transfer by diffusive convection can be important for the modification of the Atlantic layer in the central basins. The fraction of 4 W m^{-2} that can be attributed to double diffusive mixing is, however, uncertain.

[3] Relatively slow diffusion of salt, together with opposing contributions to density stratification from temperature and salinity profiles between the Arctic cold halocline layer and the core of the Atlantic layer, makes this depth segment susceptible for double diffusive convection [*Kelley et al.*, 2003]. The relative contribution of vertical temperature and salinity gradients to the stability of the water column is described by the density ratio $R_\rho = \beta\frac{\partial S}{\partial z}/\alpha\frac{\partial T}{\partial z}$, where $\alpha = -\frac{1}{\rho}\frac{\partial \rho}{\partial T}$ and $\beta = \frac{1}{\rho}\frac{\partial \rho}{\partial S}$ are the coefficients for thermal expansion and saline contraction, respectively. Double diffusive convection is expected for $R_\rho > 0$ and can be separated into two different regimes of instability; salt fingering for temperature and salinity decreasing with depth and $0 < R_\rho < 1$ and diffusive convection for temperature and salinity increasing with depth and $R_\rho > 1$. The buoyancy flux increases as R_ρ approaches 1 from above and regions with density ratios in the range $1 < R_\rho < 10$ are considered susceptible to diffusive convection [*Kelley et al.*, 2003]. The diffusive convection regime will be the main focus of this work. Salt fingering favorable stratification is widespread in

[1]Geophysical Institute, University of Bergen, Bergen, Norway.
[2]Bjerknes Centre for Climate Research, Bergen, Norway.

Corresponding author: A. Sirevaag, Geophysical Institute, University of Bergen, Allegt. 70, NO-5007 Bergen, Norway. (anders.sirevaag@gfi.uib.no)

0148-0227/12/2012JC007910

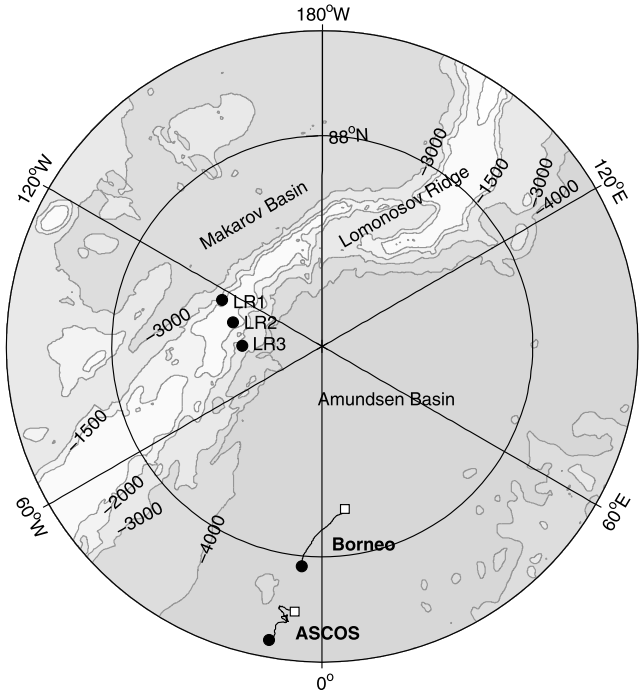

Figure 1. Map of the central Arctic Ocean showing the bathymetry of the Amundsen and Makarov Basins and the Lomonosov Ridge. The ASCOS and Borneo drifts are indicated together with the three stations (LR1-3) at the Lomonosov Ridge.

the tropical and subtropical pycnocline [*Schmitt*, 1994; *You*, 2002].

[4] A region with active diffusive convection can be characterized by a distinct staircase structure of homogenous, well mixed layers separated by relatively thin, strong gradient layers, termed *layers* and *interfaces*, respectively (see Figure 2 for an example). The vertical heat flux within a staircase is suggested to scale with the temperature difference across the high gradient interfaces [*Turner*, 1965] and parameterizations have been provided based on comprehensive laboratory experiments [e.g., *Foldvik and Rudels*, 1996; *Kelley*, 1990; *Marmorino and Caldwell*, 1976]. Well-defined staircases and diffusive convection have been observed in polar regions; in the central Arctic [*Melling et al.*, 1984; *Neshyba et al.*, 1971; *Padman and Dillon*, 1987, 1988; *Timmermans et al.*, 2008], in the Arctic boundary current [*Lenn et al.*, 2009; *Polyakov et al.*, 2011], and in the Weddell Sea [*Muench et al.*, 1990; *Robertson et al.*, 1995]. Vertical diffusive heat fluxes are estimated to be $O(10^{-2})$–$O(10^{-1})$ W m^{-2} for the central Arctic [*Neshyba et al.*, 1971; *Padman and Dillon*, 1987; *Timmermans et al.*, 2008], $O(1)$ W m^{-2} for the Arctic boundary current and the Barents Sea marginal ice zone [*Lenn et al.*, 2009; *Polyakov et al.*, 2011; *Sundfjord et al.*, 2007] and $O(1)$–$O(10)$ W m^{-2} for the Weddell Sea staircases [*Muench et al.*, 1990; *Robertson et al.*, 1995]. Vertical heat fluxes from diffusive convection are larger than those from molecular diffusion and are therefore important; however, they are at least one order of magnitude smaller than surface heat fluxes in the same areas [e.g., *Krishfield and Perovich*, 2005; *McPhee et al.*, 1999; *Sirevaag et al.*, 2010, 2011].

[5] Strong lateral temperature gradients in the Atlantic water inflow regions are suggested to develop intrusions, which are observed over large distances across the Arctic Ocean and can contribute to transfer of heat toward the surface through double diffusive convection [*McLaughlin et al.*, 2009; *Rudels et al.*, 1999]. In the vertical temperature and salinity profiles, susceptible regions for double-diffusive mixing are found around such thermohaline intrusions, where an increasing salinity and temperature has the potential for diffusive convection (typically above a warm and salty intrusion) and a decreasing salinity and temperature has the potential for salt fingering (typically below a warm salty intrusion). Such intrusions are found widespread in the Eurasian Basin [e.g., *Dmitrenko et al.*, 2008; *May and Kelley*, 2001; *Rudels et al.*, 1999].

[6] In this work, we utilize observations from microstructure profiling in the central Amundsen Basin in April and August 2008 to quantify the vertical heat transfer by diffusive convection. Using observations, we evaluate existing parameterizations for diffusive convective heat transfer based on large scale properties of the water column and we also investigate the Lomonosov Ridge as a possible formation site of thermohaline intrusions which are important for maintaining thermohaline staircases. Details on sampling, data processing, flux calculations and staircase detection are provided in section 2. Section 3 provides the general properties of the vertical ocean structure for the two surveys in consideration, while section 4 discusses the properties, variability, fluxes and parameterizations of the observed Amundsen Basin staircase. In section 5, we discuss the formation process of the observed temperature and salinity intrusions and contrast the structure in Amundsen Basin observation with that across the Lomonosov Ridge. A summary is provided in section 6.

2. Data and Methods

2.1. Microstructure Profiling

[7] Measurements of hydrographical properties and ocean turbulence were made in the upper 500 m using a microstructure profiler. Profiles were collected during two experiments carried out in 2008. The first experiment was conducted from the Russian drifting ice camp Borneo between 18 and 25 April 2008 in the Amundsen Basin (hereafter referred to as Borneo) (Figure 1). The second experiment was carried out farther south, between 15 August and 1 September 2008, during the drift of the Swedish ice breaker Oden as part of the Arctic Summer Cloud Ocean Study (hereafter referred to as ASCOS). At the end of the Borneo sampling three additional stations were occupied across the Lomonosov Ridge (LR), accessed by a helicopter on 25 April 2008 (LR1–3, Figure 1). In total 213 and 345 profiles were obtained during the Borneo and ASCOS drifts, respectively. Of the 213 Borneo profiles, the last 3 casts were across the LR and 41 casts were more frequent profiles over limited depth ranges, leaving 169 deep (500 m) casts. The water depth, however, was greater than 4000 m during both drifts. Profiles were collected, typically once every hour, in a heated tent, through a hydrohole in the ice using a motorized winch.

[8] A loosely tethered free-fall profiler MSS-90L (ISW Wassermesstechnik, Germany, MSS hereafter), was used in

both experiments. The MSS was equipped with precision conductivity, temperature, depth (CTD) sensors, two air-foil shear probes and one fast-response glass-coated bead thermistor (Thermometrics FP07) [*Fer*, 2006, 2009]. High-resolution temperature gradients were also sampled from the FP07 through a pre-emphasized channel (i.e., the sensor's output increases with the frequency in order to increase the signal-to-noise ratio [see, e.g., *Mudge and Lueck*, 1994]). All channels of the profiler, including the CTD sensors, sampled at 1024 Hz and were averaged to 256 Hz to reduce noise. Hydrographic parameters, salinity, potential temperature and potential density anomaly were obtained from the precision CTD sensors as 10 cm vertical averages, i.e., an average over 30–40 data points after correcting for the mismatch in the temperature and conductivity sensors [*Fer*, 2006].

2.2. Processing of Shear Microstructure

[9] The viscous dissipation rate of turbulent kinetic energy per unit mass, ε (W kg^{-1}), was calculated using the isotropic relation $\varepsilon = 7.5\nu\langle u_z'^2\rangle$ where ν is the viscosity of seawater, $\langle u_z'^2\rangle$ is the shear variance of the horizontal small-scale velocity and brackets indicate averaging. The shear variance was obtained by integrating the low wave number portion of the shear spectrum using 1-s long (about 0.7 m) half-overlapping segments. Unresolved shear variance in the high wave number portions, affected by noise, were accounted for using the empirical theoretical shape [*Oakey*, 1982]. The instrument fall speed ($W \sim 0.7$ m s^{-1}) inferred from the rate of change of the pressure record in each 1-s window, was used to convert data from the frequency domain to the wave number domain. Resulting ε values from both shear probes were quality screened and then averaged in 1-m vertical bins. The noise level of the shear probes in terms of the dissipation rate was about 6×10^{-10} W kg^{-1} for Borneo and 8×10^{-10} W kg^{-1} for ASCOS.

2.3. Processing of Thermal Microstructure

[10] Temperature microstructure from the pre-emphasized FP07 signal was used to measure the dissipation rate of thermal variance $\chi = 2\kappa_T\langle 3(\partial T'/\partial z)^2\rangle$, where $\kappa_T = 1.4 \times 10^{-7}$ m^{2}s^{-1} is the molecular diffusivity for heat, $\langle(\partial T'/\partial z)^2\rangle$ is the small scale temperature gradient variance, and the factor 3 follows from the assumption of local isotropy.

[11] The response of the glass bead-type thermistor is limited by diffusion and attenuation of the signal due to the boundary layer around the probe, and can be approximated by $H^2(f) = (1 + (f/f_c)^2)^{-2}$ where $f_c = 1/(2\pi\tau W^{-0.32})$, τ is the response time of the thermistor, here taken as 12×10^{-3} s, and W is the fall rate of the profiler [*Gregg and Meagher*, 1980]. The limited response of the thermistor was accounted for electronically before the signal was sent to the pre-emphasized channel where gain increases linearly from 3 dB at 1 Hz to about 30 dB at 40 Hz. The high-resolution temperature record was obtained by deconvolving the pre-emphasized signal [*Mudge and Lueck*, 1994] and then calibrating against the precision temperature profile (using a third order polynomial) for each cast. The time rate of change of the temperature was then calculated and converted to the vertical gradient of temperature $\partial T'/\partial z$, by multiplying by the fall rate of the profiler.

[12] The temperature gradient variance was obtained by spectral analysis. The MSS profiler is designed for shear microstructure measurements; hence the fall rate of the profiler was not adequate to sufficiently resolve the temperature gradient spectrum. Relatively quiescent Arctic water column, however, allows for reliable calculations since the temperature gradient spectrum is better resolved for less energetic turbulence [*Gregg*, 1999]. For the full-profile thermal microstructure analysis, we used 6-s ($\sim$4.2 m) data segments to ensure sufficient averaging of the spectra. The frequency spectrum of $\partial T'/\partial z$ was calculated and corrected for the transfer function of a first difference operator. Wave number spectrum was then obtained by scaling the frequency axis by W^{-1} and the spectral level by W, in units of cycles per meter (cpm), and variance per cpm, respectively. The temperature gradient variance was estimated by integrating the spectrum between 1 and k_{max} cpm. A suitable upper wave number, k_{max}, unaffected by noise, was chosen according to an initial estimate of χ_0, made by integrating to $k = 10/W$ cpm. k_{max} was chosen as $k_{max} = 5$ cpm if $\chi_0 \le 10^{-11}$ °C^2 s^{-1}, 10 cpm if $10^{-11} < \chi_0 \le 10^{-10}$ °C^2 s^{-1}, 20 cpm if $10^{-10} < \chi_0 \le 10^{-9}$ °C^2 s^{-1}, 30 cpm if $10^{-9} < \chi_0 \le 10^{-8}$ °C^2 s^{-1}, and 40 cpm if $\chi_0 > 10^{-8}$ °C^2 s^{-1}.

[13] The temperature gradient variance was not resolved to dissipative scales. In order to correct for the unresolved variance, we assume that the spectrum follows the universal Batchelor form [*Dillon and Caldwell*, 1980] which rolls off exponentially at the Batchelor wave number $2\pi k_B = \left(\varepsilon/\nu\kappa_T^2\right)^{1/4}$. The fraction of the unresolved variance is then k_B/k_{max}. We obtained k_B using ε measurement from shear probes and applied the correction factor k_B/k_{max} to χ. In the entire data set k_B varied between 54 and 350 cpm, with 5% and 95% quantiles of 59 and 79 cpm and a median of 64 cpm. While the temperature gradient spectrum from individual layer segments can deviate substantially from the Batchelor form, the average spectrum for the energetic temperature gradient spectra (with $\chi > 10^{-10}$ degC^2 s^{-1}) approximately follows the theoretical spectrum for wave numbers of up to 10 cpm. An independent estimate of ε from the average temperature gradient spectrum alone is identical to the shear probe measurements (averaged for the same segments). The fit to the average quiescent temperature gradient spectrum gives half the observed dissipation rate and the shape of the spectrum does not resemble the Batchelor's form. Following the analysis of *Fer* [2009], we estimate that χ and the turbulent heat flux is overestimated by up to a factor of two in segments where ε is below the noise level. The inferred heat fluxes are thus biased high and should be considered as an upper bound.

[14] In total 20654 and 41810 segments were analyzed for Borneo and ASCOS. In addition to the 6-s (4.2 m) segment full-profile processing of the thermal microstructure, a more detailed processing was conducted in the thermohaline staircase layers (section 2.6).

2.4. Eddy Diffusivity and Turbulent Heat Flux

[15] Accurate measurements of the eddy diffusivity and the turbulent heat flux are crucial for the present study. Diapycnal eddy diffusivity obtained from shear probes using the model by *Osborn* [1980] is not reliable since ε is close to the noise level in the depth range of interest (section 2.5) and the constant mixing efficiency assumption inherent in the model is not appropriate for double diffusive convection

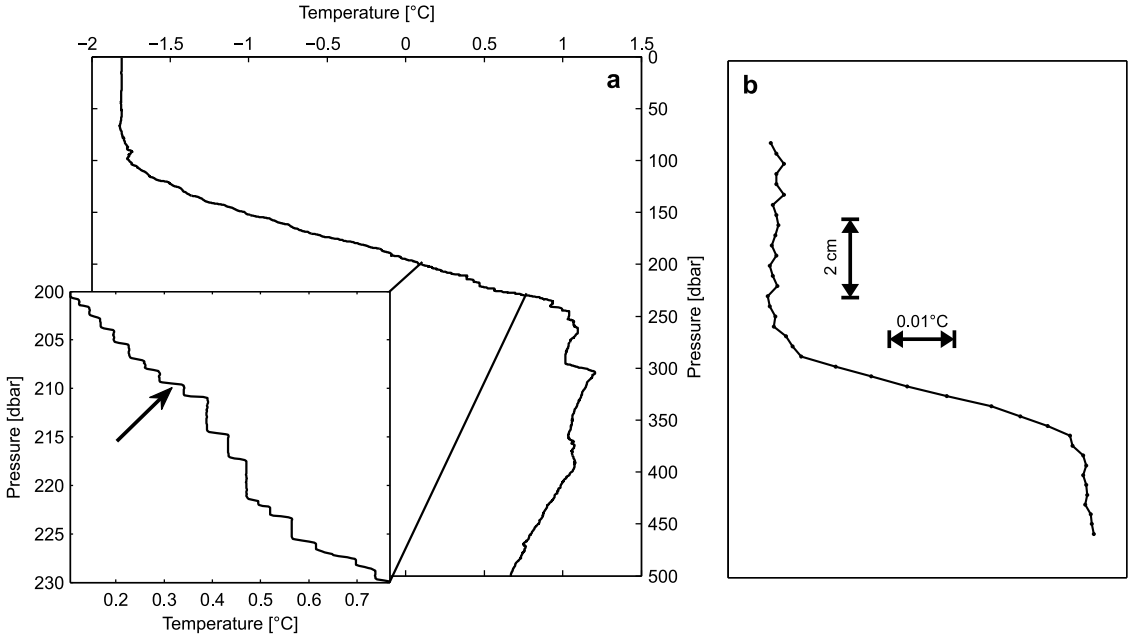

Figure 2. (a) Full temperature profile from Borneo cast 181, obtained at 88.06 N 4.40 W on 24 April 2008. Inset is a zoom-in of the 200–230 m depth range and is typical of the staircase observed above the first temperature maximum. (b) Detail of the interface identified by the arrow in the inset. Circles are full resolution (256 Hz) temperature. Vertical and horizontal scales are indicated.

[see, e.g., *Ruddick et al.*, 1997]. Instead, eddy diffusivity for heat was calculated using $K_T = \chi/2\langle\partial T/\partial z\rangle^2 \equiv 3\kappa_T c$ [*Osborn and Cox*, 1972], where $c = \langle(\partial T'/\partial z)^2\rangle/\langle\partial T/\partial z\rangle^2$ is the Cox number and $\langle\partial T/\partial z\rangle$ is the background temperature gradient over the vertical depth segment in consideration.

[16] Vertical heat fluxes from the microstructure profiles were calculated as

$$F_H = -\rho c_p K_T \left\langle \partial T/\partial z \right\rangle \tag{1}$$

where ρ and c_p is the density and specific heat within each vertical segment.

2.5. Staircase Detection and Heat Flux Within Staircases

[17] For both Borneo and ASCOS, a persistent staircase structure was observed in the depth range 200–260 m, covering the segment above the first temperature maximum (Figures 2 and 3). Step-like structures were also present above the deeper temperature maximum; however, the characteristics of these intrusive layers differed from the staircase in the 200–260 m range and are discussed separately (section 5). In each individual profile, the large scale density ratio was calculated as $\langle R_\rho \rangle = \beta\langle\frac{\partial S}{\partial z}\rangle/\alpha\langle\frac{\partial T}{\partial z}\rangle$, where $\alpha = -\frac{1}{\rho}\frac{\partial \rho}{\partial T}$ and $\beta = \frac{1}{\rho}\frac{\partial \rho}{\partial S}$ are the coefficients for thermal expansion and saline contraction, respectively and angle brackets indicate vertical averaging. Throughout this work, $\langle R_\rho \rangle$ will refer to the vertically averaged density ratio. The density ratio for individual interfaces is R_ρ as described below. In order to describe the staircase, the height of the well-mixed layers and the temperature and salinity jumps at the interfaces were quantified as follows: For each profile, the background temperature gradient in the 200–260 m depth range was calculated. A layer was defined as the portion where the local temperature gradient between adjacent data pairs was smaller than the background gradient for at least four successive points (i.e., the minimum layer height was set to 0.4 m). In order to restrict the analysis to the diffusive regime, only layers with positive T and S gradients were chosen. Adjacent layers delineate interfaces. In total 2123 interfaces were retained having positive T and S gradients with a salinity jump greater than a conservative instrumental accuracy of 0.01.

[18] The layers and interfaces meeting the above conditions were used to calculate the mean T and S of each layer. The layer height, H, was defined as the difference between the pressure reading of the upper and lower data points in a layer. Change in temperature and salinity across the interfaces, ΔT and ΔS, respectively, were calculated as the difference in temperature and salinity between neighboring layers. The density ratio across each interface is then $R_\rho = \beta\Delta S/\alpha\Delta T$.

[19] The heat flux within the staircase was estimated from a "4/3 flux law" inferred from laboratory studies [*Kelley*, 1990] (see *Kelley et al.* [2003] for a review),

$$F_{H\_K90} = \rho c_p \frac{C}{\alpha}\left(g\kappa_T^2/\nu\right)^{1/3}(\alpha\Delta T)^{4/3} \tag{2}$$

where ρ is the density, c_p is the specific heat, α is the thermal expansion coefficient, g is the constant of gravity, κ_T is the thermal diffusivity, ν is the kinematic viscosity and ΔT is the temperature difference across the interface. The flux

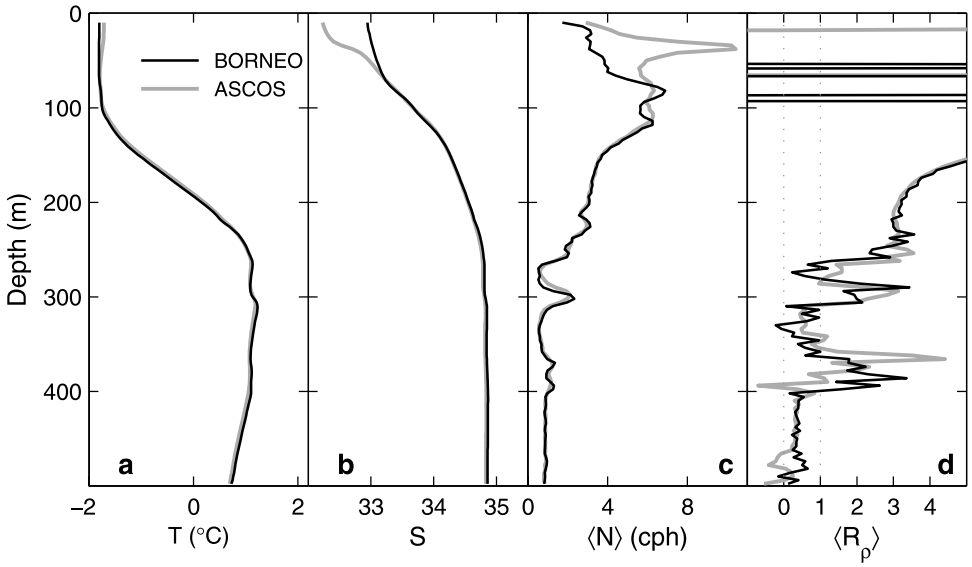

Figure 3. Survey averaged profiles of hydrographic parameters for the Borneo (black) and ASCOS (gray) drifts. For the Borneo profiles the three casts across the Lomonosov Ridge are excluded. (a) Temperature, (b) salinity, (c) buoyancy frequency, $\langle N \rangle$, in cycles per hour (cph), and (d) the density ratio, $\langle R_\rho \rangle$. The range $1 < \langle R_\rho \rangle < 10$ is susceptible to the diffusive regime of double diffusive convection, whereas salt-fingers are expected for $0 < \langle R_\rho \rangle < 1$. Both $\langle N \rangle$ and $\langle R_\rho \rangle$ are calculated as the average over the individual profiles, i.e., not using the survey mean CTD profiles.

scale factor C is a function of the density ratio, R_ρ and can be estimated by the empirical relation [*Kelley*, 1990]

$$C = 0.0032 e^{\left(4.8/R_\rho^{0.72}\right)} \tag{3}$$

where R_ρ is the density ratio across the interface. Alternative formulations of (2) and (3) are also discussed in section 4.3. All seawater properties used in the calculation of heat flux were calculated using the mean values of T and S for each interface. Salinity is given in the practical salinity scale.

2.6. Turbulent Heat Flux Calculations in Layers

[20] To the extent the measurements allow, the high-resolution T profiles are used to compare observations of heat fluxes in the staircase to the laboratory flux laws. In addition to the 6-s (4.2 m) segment full-profile processing of the thermal microstructure, a more detailed processing and analysis was conducted in the homogeneous thermohaline staircase layers. To this end, T data segments were extracted from each individual layer detected in the 200–260 m depth range (section 2.5). Spectral analysis of these segments was then performed as described in section 2.3.

2.7. Molecular Heat Flux Calculations at Staircase Interfaces

[21] The molecular diffusion of heat within each interface is estimated using the high resolution FP07 temperature signal. The average temperature spectrum from the interfaces shows that noise dominates after 30 Hz. The temperature record is therefore low-pass filtered with a cut-off frequency of 30 Hz. At a fall speed of 0.6 m s^{-1} this corresponds to smoothing at ~2 cm scale. Within an interface, heat transfer will be dictated by the largest heat fluxes; hence we used the largest detected negative temperature gradient within each interface to estimate

$$F_{Hmol} = -\rho c_p \kappa_T \left\langle {}^{\partial T}/_{\partial z} \right\rangle_{\max}. \tag{4}$$

[22] An example of the full resolution temperature data across an interface is shown in Figure 2b. When the full resolution temperature data are used to calculate the molecular fluxes, the difference resulting from using the low-pass filtered signal is marginal.

3. Oceanographic Setting

[23] Average profiles of hydrographic and mixing parameters are presented to provide the background conditions for the turbulent mixing, diffusive layering and the observed vertical heat transfer. The survey-averaged profiles of temperature, salinity, buoyancy frequency and density ratio are shown for both the Borneo and ASCOS drifts in Figure 3. The Borneo and ASCOS experiments were performed in April and August, respectively (section 2.1) and the differences in the mixed layer properties were discussed in detail in *Sirevaag et al.* [2011]. Below the mixed layer, both surveys showed a similar vertical structure with the cold halocline layer, followed by a temperature increase toward the warm Atlantic Water layer, until the first local temperature maximum at about 260 m. Thereafter temperature decreased with depth, interrupted by two inversions, one near the temperature maximum at around 310 m and a deeper one around 400 m. The increasing salinity with depth provided stability for the depth segments with temperature inversions.

[24] Buoyancy frequency, $\langle N \rangle = \sqrt{-{}^{g}/_{\rho_0} \left\langle {}^{d\rho}/_{dz} \right\rangle}$, approximated using the sorted potential density profiles, shows that

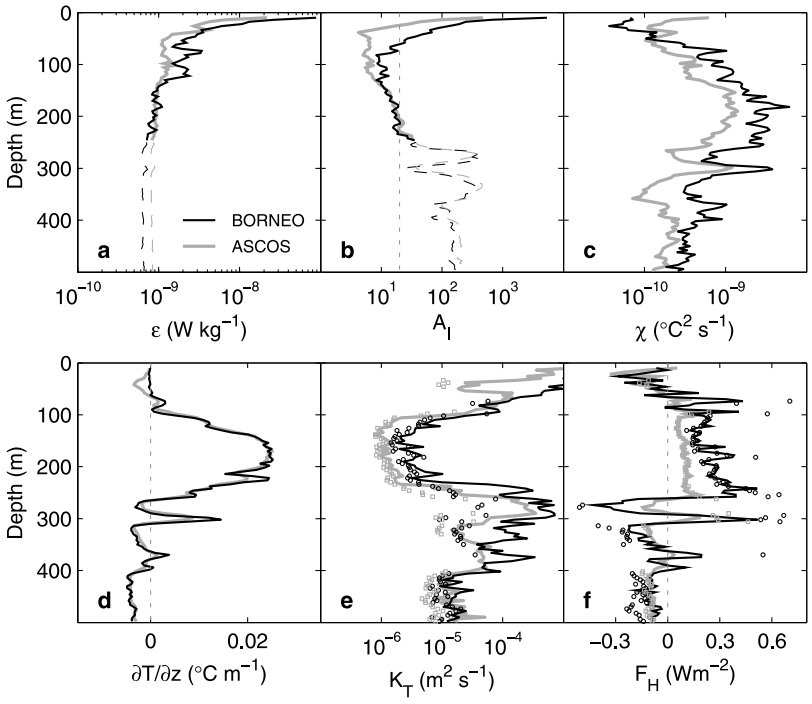

Figure 4. Survey-averaged profiles of mixing parameters for the Borneo (black) and ASCOS (gray) drifts. For the Borneo profiles the three casts across the Lomonosov Ridge are excluded. (a) Dissipation rate of TKE, ε, (b) turbulent activity index, $A_I = \varepsilon/\nu N^2$, (c) dissipation rate of temperature variance, χ, (d) mean vertical temperature gradient, (e) eddy diffusivity for heat, K_T, and (f) the vertical heat flux, F_H. Profiles are averaged over individual casts processed using 6-s (4.2-m) length segments. Additionally, eddy diffusivity and heat flux profiles obtained using the average χ and the average temperature-gradient profiles are shown by circles. The thin, dashed portions in Figures 4a and 4b mark the depth range where ε is near the noise level of the profiler. The vertical dashed line in Figure 4b marks $A_I = 20$ below which the turbulence, if any, is anisotropic and also cannot induce a net vertical buoyancy flux, i.e., cannot cause diapycnal mixing.

the least stable part of the profiles were the segments in between the temperature maxima (Figure 3c). These quasi-homogenous layers had a density ratio, R_ρ, typically between 0 and 1, susceptible for salt fingering (Figure 3d). Depth segments with $1 \le R_\rho \le 10$ are considered to be susceptible for double diffusive layering with stronger convection for small R_ρ; above the temperature maxima R_ρ was typically less than 4 for both Borneo and ASCOS (Figure 3d). The persistent staircase was observed in the depth range 200–260 m above the temperature maximum at all casts (see Figure 2 for an example), however, it was smoothed out in the average profile (Figure 3a). The decreasing salinity with depth below 400 m, susceptible for salt-fingering, is not visible due to the large vertical scale on the figure.

[25] Average profiles for the mixing parameters are shown in (Figure 4). Below a turbulent upper layer of about 50 m the Arctic water column is quiescent. Dissipation rates of turbulent kinetic energy (TKE) were largest in the mixed layer and decreased rapidly toward the noise level of the profiler (Figure 4a), which was reached below ~260 m, i.e., just below the staircase. From the average profiles of dissipation rate of TKE and buoyancy frequency, the turbulent activity index, $A_I = {}^{\varepsilon}/_{\nu N^2}$ was calculated. A_I indicates the strength of the turbulence relative to stratification and when $A_I \le 20$ (the threshold is approximate and uncertain) turbulence is too weak to induce a net vertical buoyancy flux in a stratified flow [*Thorpe*, 2005]. Average Borneo and ASCOS profiles indicated A_I below or around this threshold below the mixed layer (Figure 4b), suggesting negligible diapycnal mixing. Below 150 m depth, ε profile is strikingly similar at both sites (except that noise level is slightly higher for ASCOS). Between 150 and 250 m, the dissipation rate of TKE was identical to within 20% for the two drifts. Above 150 m, Borneo was approximately 3 times more turbulent, presumably as a result of relatively stronger atmospheric forcing in April compared to August. The relatively energetic upper layer during April is not reflected in the temperature structure in the mixed layer: the dissipation rate of temperature variance, χ, in the upper 50 m was a factor of 3 larger during ASCOS, presumably because the temperature in the upper 50 m was isothermal during Borneo and the thermodynamic forcing was larger in August. Below this upper layer χ was, on the average, 3 times larger during Borneo (Figure 4c), however both surveys showed elevated χ in the depth range with the strongest temperature gradient (~100–250 m).

[26] Eddy diffusivity for heat, K_T, calculated as described in section 2.4 (Figure 4e) was used together with temperature gradient profiles (Figure 4d) to calculate vertical heat fluxes, F_H, (Figure 4f) according to (1). The difference between Borneo and ASCOS in the average profiles of K_T and F_H mainly stems from the difference in χ profiles. The

Table 1. Mean and Standard Deviation of Staircase Properties From Borneo and ASCOS Profiles

	Borneo	ASCOS
n-layers	1179	2502
n-interfaces	680	1443
H [m]	1.35 ± 1.49	1.20 ± 1.10
ΔT (°C)	0.065 ± 0.024	0.061 ± 0.019
ΔS	0.016 ± 0.005	0.015 ± 0.004
R_ρ	3.0 ± 0.4	3.0 ± 0.3
F_{H_K90} (W m^{-2})	0.65 ± 0.42	0.55 ± 0.27

mid-depth values of enhanced eddy diffusivity between 250 and 400 m cover the portions of the profiles characterized by salt fingering and the intrusions. Averaged below 400 m depth, $K_T = 1.9\ (\pm 0.8) \times 10^{-5}$ m^2 s^{-1}, corresponding to a Cox number of $c = 45$. The stability density ratio, R_ρ was 0.35 ± 0.15.

[27] Our results in the salt-fingering favorable stratification below 400 m can be compared to the observations conducted in the Caribbean-Sheets and Layers Transects (C-SALT) experiment in the thermohaline staircase in the western tropical North Atlantic [*Schmitt et al.*, 1987]. In the C-SALT staircase characterized by $R_\rho \sim 0.6$, *Gregg and Sanford* [1987] obtained c $\sim$ 88 (after dividing by the factor 3 difference in our definitions), suggesting salt fingering might be significant below the AW core in determining the eddy diffusivity. The measurement and processing uncertainties inherent in microstructure data aside, the factor of two difference in c between our observations and that in C-SALT staircase could be attributed to relatively large shears encountered in the C-SALT interfaces [*Kunze*, 1994].

4. Amundsen Basin Thermohaline Staircase

[28] The staircase detection criteria given in section 2.5 were applied on all profiles collected during the Borneo and the ASCOS experiments. In total, 1179 and 2502 layers were identified for the Borneo and ASCOS profiles, respectively, and the corresponding numbers of interfaces were 680 and 1443. Mean properties of layers and interfaces for the 200–260 m depth segment are given in Table 1.

4.1. Staircase Overview

[29] In the staircase depth range, the background temperature and salinity stratification was similar with $\langle R_\rho \rangle = 3$ on average (Figures 3a and 3b). The higher dissipation rate of thermal variance, χ found during Borneo leads to enhanced background eddy diffusivity and turbulent heat flux compared to ASCOS.

[30] Staircase properties were similar for the two drifts (Table 1). The average (integer) number of detected layers in a single profile was 7 for both surveys. The average layer height was slightly larger for Borneo than ASCOS (1.35 m vs 1.20 m). Average change in temperature and salinity across the interfaces was also slightly larger for Borneo than ASCOS, however the average layer density ratio was similar for both experiments. A larger temperature change across the interface is also reflected in a larger average heat flux (derived using the laboratory flux law) for Borneo than ASCOS (0.65 W m^{-2} versus 0.55 W m^{-2}).

[31] Early observations in the Canada Basin staircase [*Neshyba et al.*, 1971], revealed layers that were two to three times thicker, but with interface ΔT three times smaller than we observe in the Amundsen Basin. *Padman and Dillon* [1987] reported similar figures in 1985, however *Timmermans et al.* [2008] reported generally thicker layers from observations in 2004–2007, with ΔT ($\sim$0.04°C) similar to our observations. Although not conclusive, *Timmermans et al.* [2008] suggested that higher ΔT could be a result of the recent warming and shoaling of the Atlantic Layer in the Canada Basin.

4.2. Staircase Variability

[32] Distributions of layer and interface characteristics are shown in Figure 5. The staircases observed in Borneo and ASCOS were not only similar in mean values, but also in distribution. The observed layer and interface characteristics show that the observed Amundsen Basin staircase is consistent throughout the study region and through different seasons. Approximately 40% of the detected layers had thicknesses between 0.4 and 0.7 m, but a relatively long tail in the distribution affected the average thickness (Figure 5a). Layers were detected in the entire depth range considered, with a small peak in occurrence near 225 m depth (Figure 5b). When comparing ΔT and ΔS across interfaces (Figure 5c and Figure 5d), there was a slight shift in distribution toward higher values for the Borneo profiles compared to ASCOS. This was also reflected in heat fluxes (Figure 5f) where the distribution of Borneo interface heat fluxes was wider than the relatively narrow distribution of heat fluxes during ASCOS, reflecting a larger variability during the Borneo survey possibly due to the larger horizontal area covered by the drift. The interface density ratio showed a narrow peak in distribution around $R_\rho = 3$ for both surveys, which is considered to be highly unstable for double diffusive convection [*Kelley et al.*, 2003].

[33] Following *Padman and Dillon* [1987], we examine the vertical distribution of layers and interfaces by averaging the staircase properties in 10-m depth intervals (Table 2). Density ratio and the buoyancy frequency are segment averages over the 10-m depth range in consideration. In general, the layer height increased from less than 1 m at 200 m depth to well above 2 m at 260 m depth. There was a slight decrease in interface ΔT and ΔS with depth; however $\langle R_\rho \rangle$ remained relatively constant which shows that the changes in large-scale gradients in T and S compensated. Buoyancy frequency and interface heat flux decreased toward the lower part of the 200–260 m depth interval. The observed vertical variability was similar to that in the Canada Basin thermohaline staircase with respect to layer height and changes in interface ΔT, ΔS and the vertical heat flux [*Padman and Dillon*, 1987].

[34] One of the characteristics of a staircase is its lateral coherence and extent [*Kelley et al.*, 2003]. By plotting temperatures and salinities of individual layers in a *T-S* diagram, *Timmermans et al.* [2008] identified the thermohaline staircase within the Canada Basin over an area stretching several hundreds of kilometers. *Padman and Dillon* [1988] used a different approach, where they compared a sequence of temperature profiles and determined coherency by tracking the vertical position of individual layers. However, they found that this method required high resolution lateral sampling with less than 15 m separation between neighboring profiles and were only able to trace

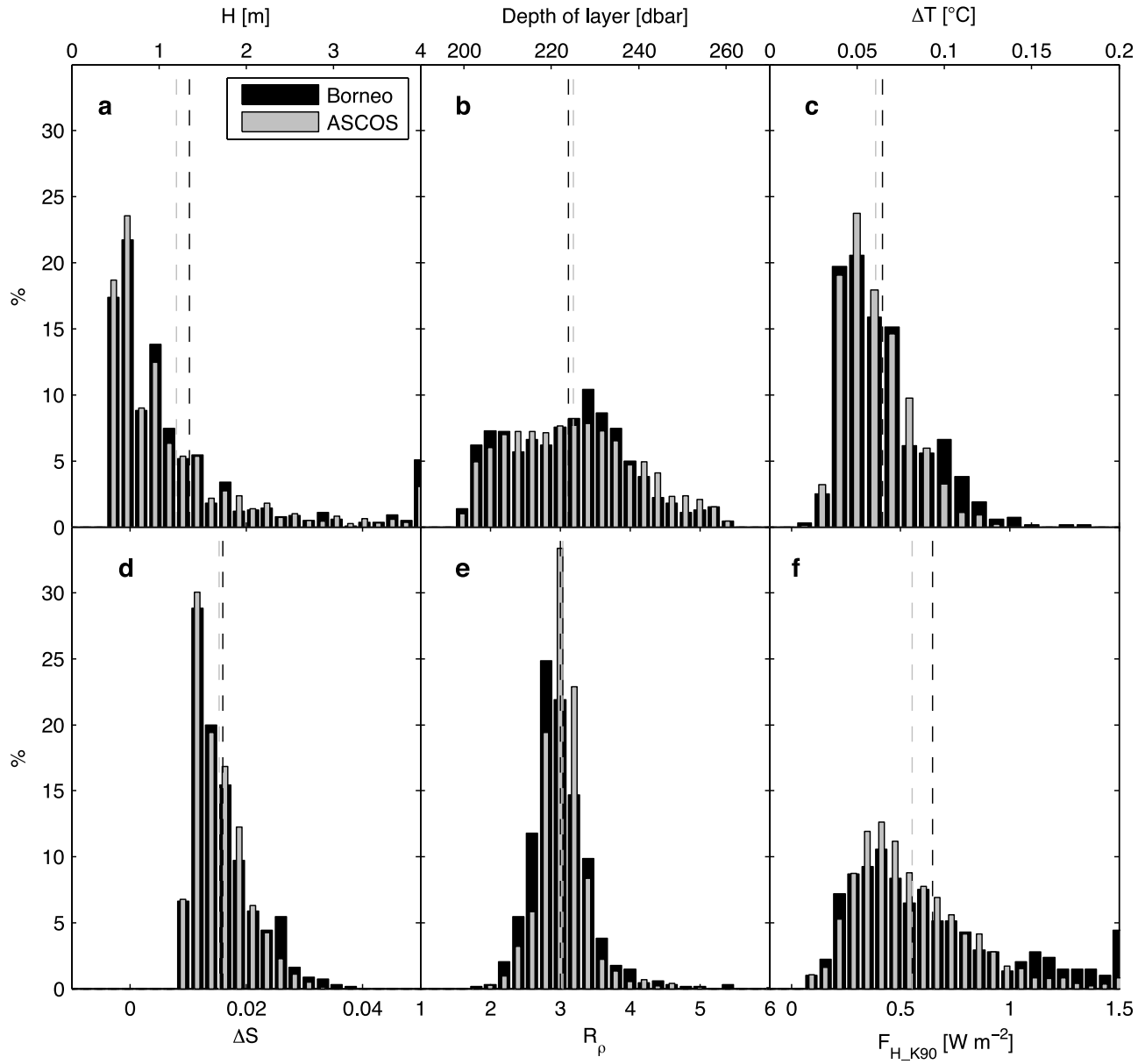

Figure 5. Histograms of layer and interface characteristics for the 1179 and 2502 layers detected in the Borneo and ASCOS profiles, respectively. Distributions show (a) layer height H, (b) depth where layers are detected, (c) temperature change ΔT across interfaces, (d) salinity change ΔS across interfaces, (e) density ratio calculated from ΔT and ΔS, and (f) the vertical heat flux across the staircase as calculated by (2).

Table 2. Mean Properties of Layers and Interfaces Averaged in 10 m Depth Intervals for the ASCOS and Borneo Field Profiles[a]

	Borneo							ASCOS						
Depth Interval	n	H (m)	ΔT (°C)	ΔS	$\langle R_\rho \rangle$	$\langle N \rangle$ 10^{-3} s^{-1}	F_{H_K90} (W m^{-2})	n	H (m)	ΔT (°C)	ΔS	$\langle R_\rho \rangle$	$\langle N \rangle$ 10^{-3} s^{-1}	F_{H_K90} (W m^{-2})
200–210	241	0.97	0.065	0.015	3.1	5.2	0.61	436	0.94	0.064	0.015	3.1	5.0	0.55
210–220	230	1.03	0.067	0.016	3.1	4.8	0.67	554	0.92	0.065	0.016	3.0	4.8	0.62
220–230	316	1.00	0.067	0.017	3.0	5.3	0.70	604	0.98	0.065	0.017	3.1	5.1	0.59
230–240	257	2.07	0.063	0.017	3.4	4.6	0.62	484	1.27	0.059	0.016	3.1	4.4	0.55
240–250	87	2.65	0.060	0.015	3.7	3.6	0.65	282	1.94	0.049	0.013	3.3	3.7	0.45
250–260	48	3.07	0.051	0.013	4.0	3.5	0.55	142	3.04	0.044	0.013	3.0	3.4	0.41

[a]Density ratio $\langle R_\rho \rangle$ and buoyancy frequency $\langle N \rangle$ are segment averages over the given depth interval.

Table 3. Statistics of Background Mixing Parameters in the Layers in the Thermohaline Staircase Range, 200–260 m[a]

	Mean	STD	MLE	Lower	Upper
χ (10^{-10} °C^2 s^{-1})	4.1	5.9	3.9	3.7	4.1
ε (10^{-10} W kg^{-1})	9.4	5.4	9.3	9.2	9.5
A_I	53.8	45.7	53.3	51.9	54.8
c	6.7	21.4	4.8	4.5	5.1
K_T (10^{-6} m^2 s^{-1})	2.8	9.0	2.0	1.9	2.1
F_H (W m^{-2})	0.08	0.13	0.07	0.07	0.07
Γ	0.05	0.14	0.05	0.04	0.05

[a]Parameters are the dissipation rate of temperature variance, χ, dissipation rate of TKE, ε, turbulent activity index, A_I, Cox number, c, eddy diffusivity for heat, K_T, vertical heat flux (+ve upward), F_H, and the dissipation ratio, Γ. Statistics shown are the mean and standard deviation (STD), the maximum likelihood estimator from a lognormal distribution (MLE) and the 95% lower and upper confidence intervals of MLE.

individual layers laterally for up to 600 m. We applied both methods and found no significant lateral coherency in the observed staircases (not shown). The signatures of individual layers in a *T-S* diagram as reported in other studies [e.g., *Polyakov et al.*, 2011; *Timmermans et al.*, 2008] were not detectable, but in some cases a pattern of a staircase can be identified in up to five profiles in a row, however no systematic horizontal coherence beyond this was found. The lack of horizontal coherence of layers can be attributed to several factors. For Borneo and ASCOS, average distance between neighboring profiles was 400 and 270 m, respectively, which is comparable to the distance where the layers in the Canada Basin staircase lose coherence [*Padman and Dillon*, 1988]. Heat fluxes are in general larger than those observed in the Canada Basin which will modify the layers quicker leading to convection, formation of intermediate layers and removal of interfaces. Also, processes associated with internal wave breaking or near inertial oscillations could induce mixing and reduce the horizontal continuity in layers.

4.3. Interface Heat Fluxes

[35] In a well-developed staircase, heat transfer is provided by molecular diffusion in the strongly stratified, laminar interfaces and by turbulent convective mixing in the well-mixed, homogeneous layers. Parameterizations of the double diffusive heat fluxes are developed to estimate fluxes based on the large scale gradients in the vertical temperature profile. In order to evaluate heat fluxes estimated by (2), we compare F_{H_K90} with turbulent heat fluxes F_H and molecular heat fluxes F_{Hmol}, as described in section 2.6. For the comparison, F_H in a layer is assigned to the nearest interface below. An overview of background mixing parameters in the 200–260 m range is provided in Table 3.

[36] The distribution of the F_H is shown in Figure 6 together with the distribution of F_{H_K90} and molecular fluxes, F_{Hmol}. Average F_H was 0.07 ± 0.09 W m^{-2}, an order of magnitude smaller than average F_{H_K90}, which might indicate that the parameterization of diffusive convective fluxes overestimated the vertical heat transfer in the diffusive staircase. The discrepancy between the observed and parameterized fluxes is discussed in section 4.4. Molecular fluxes were of the same order as F_H, with an average value of 0.05 ± 0.04 W m^{-2} for both the Borneo and ASCOS survey (Figure 6) and with a similar distribution. Although fluxes up to 1 W m^{-2} were estimated for some interfaces, more than 70% of the fluxes were between 0 and 0.08 W m^{-2}.

[37] The slight shift toward higher values in the distribution of turbulent heat fluxes, F_H, compared to molecular fluxes might be due to 1) enhanced turbulence in the staircase depth segment 2) deviation from isotropy and 3) an overestimation of K_T to calculate F_H. Enhanced turbulent mixing can be caused by shear or internal waves and might be visible as a larger temporal variability in the staircase structure. Attempts to track individual layers and interfaces within the staircase failed possibly due to a significant splitting and merging of layers and interfaces. This indicates additional processes besides double diffusive mixing. Calculation of turbulent fluxes assumes local isotropy which is violated in the presence of strong layering. Relatively strong stable stratification of layers can lead to anisotropy down to viscous scales allowing only vertical gradients of horizontal velocity to persist leading to $\varepsilon \sim 2\nu\langle u_z'^2\rangle$, i.e., a factor of 3 less than the isotropic relation [*Denman and Gargett*, 1988]. Turbulent fluxes are then overestimated by a factor of 3. Also, the eddy diffusivity is obtained from temperature gradient variance, which is corrected for the unresolved variance using the Batchelor wave number calculated from ε measured by the shear probes (section 2.3). Because ε is close to the noise level, this correction might lead to overestimated eddy diffusivity (hence overestimated F_H).

[38] Turbulent heat fluxes, F_H were of similar magnitude and distribution for the Borneo and ASCOS surveys and hence might represent a quantification of vertical heat fluxes due to double diffusive convection in the Amundsen Basin. Although F_{H_K90} is significantly larger, F_H is of similar

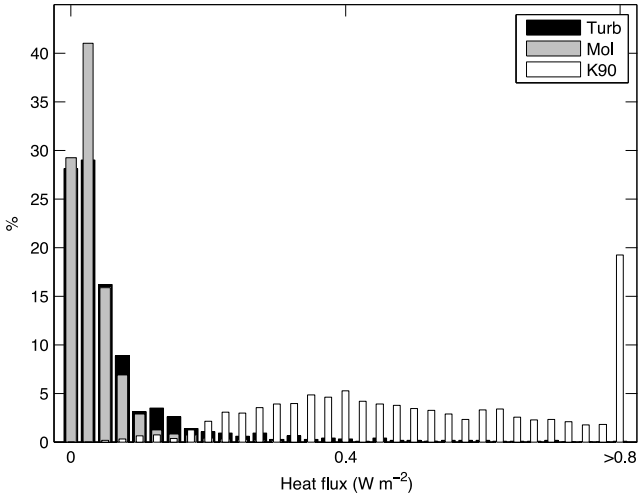

Figure 6. Heat fluxes from parameterization of diffusive convection (K90) estimated from (2), turbulent heat fluxes (Turb) calculated over layers and molecular heat fluxes (Mol) through the interfaces calculated from the interface temperature gradient detected by high resolution temperature according to (4). All heat fluxes are calculated using both Borneo and ASCOS profiles.

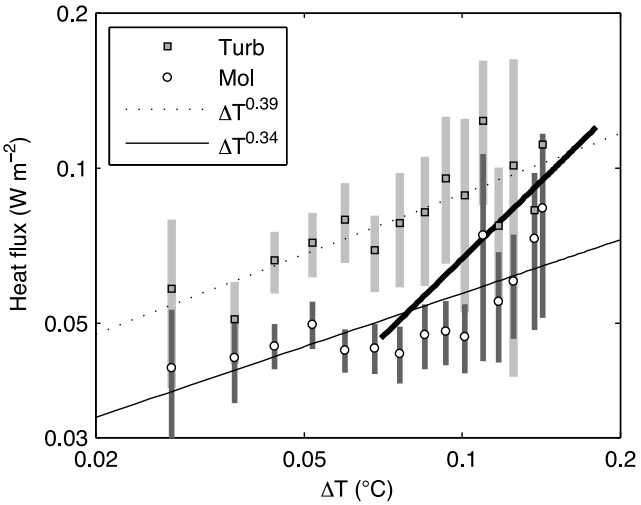

Figure 7. Interface heat fluxes plotted against the interface temperature change. Fluxes shown are the molecular heat flux (Mol), turbulent heat fluxes in adjacent layers (Turb) and exponential fits to both turbulent (dashed line) and molecular (solid) fluxes. Error bars on flux estimates indicate the standard error and the thick, solid line shows $\Delta T^{4/3}$ dependence for reference.

magnitude as observed in other areas of the Arctic. In the Canada Basin, double diffusive heat fluxes were found to be in the range of 0.02–0.1 W m^{-2} [*Padman and Dillon*, 1987], using a heat flux parameterization from *Marmorino and Caldwell* [1976] instead of the parameterization from *Kelley* [1990] as used in this study. Based on more recent observations from the Canada Basin, *Timmermans et al.* [2008] found vertical heat fluxes to be 0.05–0.3 W m^{-2} and values were consistent using both parameterizations, although a significant lateral variability was detected. In the Eurasian Basin, *Lenn et al.* [2009] inferred double diffusive heat fluxes of ~1 W m^{-2} in the boundary current along the continental shelf of the Laptev Sea.

4.4. Diffusive Layering Parameterizations

[39] An aim of performing laboratory experiments and studying the detailed properties of thermohaline staircases is to relate the small-scale properties and fluxes to the large-scale properties in order to quantify fluxes from general ocean observations. We investigate how the observed vertical heat fluxes and layer height from the Borneo and ASCOS surveys scale with parameterizations based on laboratory results.

[40] Parameterizations of the vertical heat flux within thermohaline staircases often assume that the flux is proportional to the 4/3 power of the temperature difference across an interface [*Turner*, 1965]. The "4/3 flux law" has been evaluated based on laboratory experiments. As reviewed in *Kelley et al.* [2003], layer-based flux laws for the salt finger case contradicted the oceanographic observations during the C-SALT experiment: laboratory based estimates were larger by a factor 30. For the diffusive case, limited observations broadly agree with the range inferred from flux law [*Melling et al.*, 1984; *Padman and Dillon*, 1987], but the comparisons are crude. *Kelley* [1990] emphasizes to exercise caution in using the 4/3 law, since the theory states that a more appropriate power should be closer to 5/4 (see also the thorough discussion in *Kelley et al.* [2003]). When the typical oceanic Rayleigh numbers are considered, the error in the power law leads to 30–40% overestimated diffusive fluxes [*Kelley*, 1990; *Kelley et al.*, 2003] which therefore does not cause major problems in oceanographic applications.

[41] At each interface, turbulent heat flux F_H in the adjacent layer, maximum molecular heat flux F_{Hmol} and temperature difference ΔT, are available from our observations which allow for a test of the $\Delta T^{4/3}$ dependence. Heat fluxes, averaged in $\Delta T = 5$ mK bins, are plotting against the interface temperature change ΔT (Figure 7) together with a linear regression of F_H and F_{Hmol} versus ΔT. Despite large scatter and uncertainties, both F_H and F_{Hmol} demonstrate a similar ΔT dependence for the ΔT range under consideration although F_{Hmol} is ~30% smaller in magnitude. As discussed in section 4.3 turbulent fluxes should be considered as upper bounds. The linear regression of both fluxes deviates from the laboratory based $\Delta T^{4/3}$ dependence, although the uncertainty and scatter in the upper ΔT range cannot exclude this dependence conclusively. The deviation from the laboratory based flux law can have several explanations. First, it is possible that we were not able to resolve the vertical heat fluxes for small ΔT, since the measurements are pushing the limits of our instrument and the assumptions involved (such as isotropy). However, levels of χ are above the noise level in the staircase (marginally so for ε) and the temperature gradient spectra are of reasonable quality (not shown). Second, for some of the thinnest detected layers only a small segment of data is available and a larger uncertainty in fluxes might be expected. The third possibility is that the 4/3 flux law is inadequate, especially for weak ΔT forcing.

[42] In addition to the ΔT dependence, heat fluxes vary with R_ρ through the flux scale factor C given in (3) which has been determined empirically from laboratory data. In Figure 8a, estimated heat fluxes, both turbulent and molecular, were used to calculate the numerical value of C for given density ratios, R_ρ and compared to the existing parameterizations of C by *Kelley* [1990], *Marmorino and Caldwell* [1976] and *Foldvik and Rudels* [1996]. Observations suggest a pattern which is different from the laboratory-derived curves: for low R_ρ, the flux scale factor is up to an order of magnitude smaller than (3), but within the same magnitude for the upper range of R_ρ. For $R_\rho > 3.5$, C is within a factor of two of the laboratory derived line of *Kelley* [1990]. According to (2), diffusive convective heat fluxes vary linearly with C and parameterized fluxes should be significantly larger for the lower R_ρ range. This is also the case; the ratio F_{H-k90}/F_H is 7 and 18 for $R_\rho > 3.5$ and $R_\rho < 3.5$, respectively, hence the agreement is better in the higher range of R_ρ. Note that the agreement between oceanographic observations and the laboratory-flux laws reported by *Padman and Dillon* [1987] for the Canada Basin staircase where $R_\rho = 4.9$ is consistent with our results. *Kelley* [1984, 1990] found that an effective diffusivity for diffusive convective fluxes can be provided by

$$K_{T\_eff} = CRa^{1/3}\kappa_T \tag{5}$$

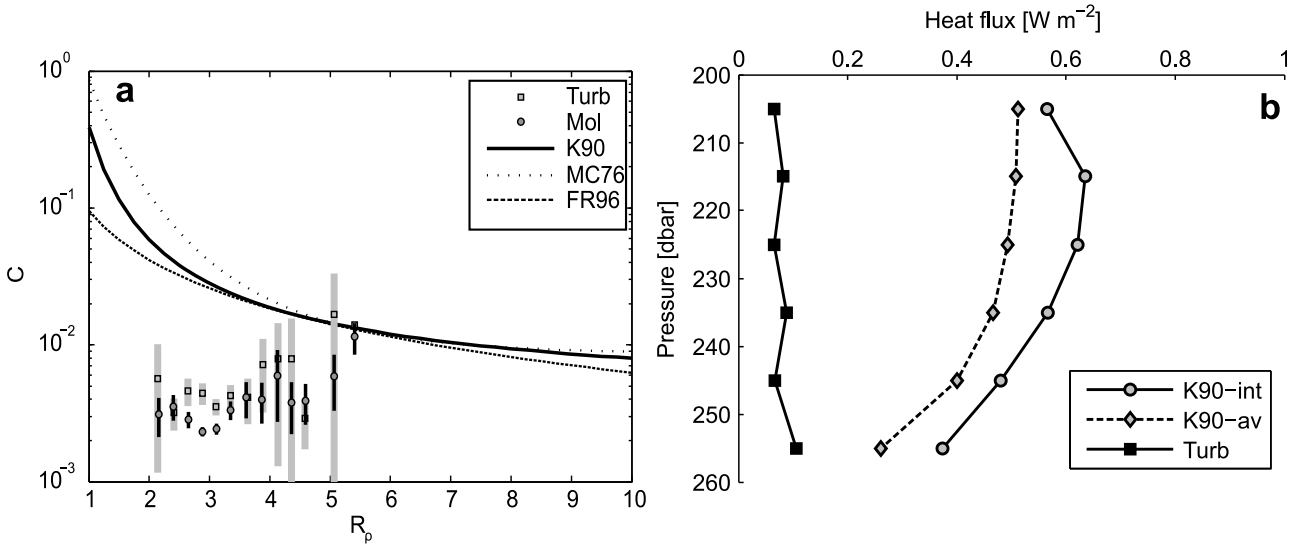

Figure 8. (a) Flux scale factor $C(R_\rho)$ calculated from (2) using the measured turbulent and molecular heat fluxes. Error bars indicate the standard error of the mean for C based on the observed fluxes. Lines indicate the parameterization of *Kelley* [1990] (K90), *Marmorino and Caldwell* [1976] (MC76) and *Foldvik and Rudels* [1996], which are based on laboratory observations. (b) Vertical heat fluxes averaged in 10 m depth segments. Fluxes are calculated according to (2) for properties of each individual detected interface (K90-int), according to (2) for vertical average 10 m properties of interface temperature change ΔT and background density ratio, R_ρ (K90-av) and from thermal microstructure, as described in section 2.4, for the thermohaline staircase layers (Turb).

where Ra is the Rayleigh number and κ_T is the molecular diffusivity of heat. Rayleigh number was estimated as $Ra = g\alpha\Delta TH^3/\nu\kappa_T$ using average staircase properties (Table 1). The layers height, H, and temperature change at the interface, ΔT, are calculated as described in section 2.5. This approach predicts ${}^{K_{T-eff}}/_{\kappa_T} \approx 19$ for an average R_ρ of 3. Observed eddy diffusivity yields ${}^{K_T}/_{\kappa_T} \approx 16$. Compared to observations, (5) thus overestimates the eddy diffusivity, not inconsistent with the overestimated flux ratio C.

[43] Another key variable for the scaling and parameterization of the staircase layers and interfaces is the layer height. *Ruddick and Turner* [1979] suggested that the layer height within a thermohaline staircase was determined by variations in salinity and temperature across a horizontal front and the buoyancy frequency. On the other hand, *Kelley* [1984] derived from dimensional analysis that the layer height was not set by larger scale horizontal gradients, but was a function of the vertical density ratio R_ρ, buoyancy frequency, molecular viscosity and diffusivity for heat and salt. The layer height was given as

$$H = GH_0 = G\left({}^{\kappa_T}/_{\langle N\rangle}\right)^{1/2} \tag{6}$$

where $\langle N\rangle$ is the buoyancy frequency averaged over the vertical segment in consideration and the scaled layer height, G, is a function to be determined empirically from observations. H_0 is a thickness layer scale defined as given in (6) [*Kelley*, 1984]. Using best fit to observations for R_ρ between 1 and 8, *Kelley* [1984] obtained

$$G = \left[RaPr\left(R_\rho - 1\right)\right]^{1/4} \tag{7}$$

where $Pr = {}^{\nu}/_{\kappa_T}$ is the Prandtl number and the Rayleigh number is approximated as $Ra = 0.25 \times 10^9 R_\rho^{1.1}$.

[44] Layer and interface properties averaged in 10-m depth segments from 200–260 m (Table 2) were used to calculate a modified scaled layer height

$$G_* = {}^{H}/_{H_0 Pr^{1/4}} \tag{8}$$

removing the Prandtl number dependence [*Padman and Dillon*, 1987]. G_* is a function of H and $\langle N\rangle^{1/2}$ and we estimated the standard error of the mean by considering the propagation of error from two independent variables as [e.g., *Emery and Thomson*, 2001]:

$$\delta G_* = \frac{G_*}{\sqrt{n}}\left[\frac{\sigma_H^2}{H^2} + \frac{\left(\frac{1}{2}\sigma_N\right)^2}{\langle N\rangle}\right]^{1/2} \tag{9}$$

where σ is the standard deviation and n is the degrees of freedom. Due to the lack of lateral coherence (section 4.2) we assume that every fifth profile is independent and approximated n by the number of data points in each segment divided by five. The variation of G_* with ratio R_ρ is shown in Figure 9 together with the estimated errors.

[45] The agreement between the observed and theoretically scaled layer height is reasonably good (Figure 9). However, the resulting scaled layer height cluster in two groups for both the Borneo and ASCOS survey; one group with $G_* \sim 100$ and $R_\rho \sim 3$ with small error and another group with higher G_* and R_ρ between 3 and 4. The latter group is in closer agreement with the theoretical estimate given by (8). The G_* estimates in the first cluster are all from the upper parts of the depth range considered (200–230 m

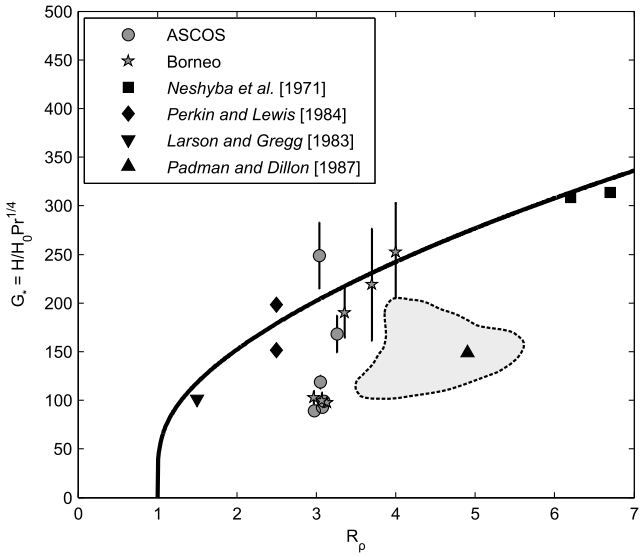

Figure 9. Scaled layer height G_* for ASCOS and Borneo individual 10 m layers (filled circles and stars). Error bars are ± 1 standard error of the mean. Solid line is the relation suggested by *Kelley* [1984]; shaded area indicates the range of G_* for the Canada Basin staircase [*Padman and Dillon*, 1987].

for Borneo and 200–240 m for ASCOS), hence the layers detected in the lower part of the staircases, closest to the temperature maximum, agree better with the theoretical scaled layer height. These layers in general display thicker layers (larger H), weaker stability (smaller N) and, for Borneo only, higher density ratios (R_ρ). The cluster of layer heights with R_ρ around 3, where the layer scaling deviates from the parameterization, also coincides with the part of the staircase where the observed flux ratios and effective diffusivities deviate the most from the parameterized values. If small steps are present in ocean observations, but not in the laboratory experiments, parameterization might not be relevant for certain ranges of a staircase and fluxes might be overestimated. *Kelley et al.* [2003] discuss this shortcoming of the parameterization, e.g., the splitting and merging of layers observed in ocean are not accounted for by the parameterization.

[46] A timely question which has been addressed in most studies dealing with double diffusive fluxes, is whether a 4/3 flux law is appropriate or valid for oceanographic cases. Both *Kelley et al.* [2003] and *Kelley* [1990] discussed the parameterization and suggest that although the parameterization is principally not correct for ocean staircases, it can be used for oceanographic studies with an error of about 30–40%. Figure 8b shows a comparison of 10-m bin-averaged turbulent fluxes (Turb) and fluxes parameterized from (2) based on interface properties (K90-int) and on 10 m vertically averaged values of ΔT and R_ρ (K90-av). From (2), fluxes are overestimated by more than a factor of 5 in the upper part of the staircase, where layers in general are thin and density ratios are low. This contradicts the 30–40% error stated above. Furthermore, observed turbulent fluxes were relatively constant with depth, whereas the parameterized fluxes decreased with depth implying a heat flux divergence within the staircase, which is likely an artifact of the parameterization.

5. Amundsen Basin Intrusion Properties

[47] In the Arctic Ocean water column, inversions in temperature and salinity can often be observed which form layering structures, so-called intrusions. *Rudels et al.* [1999] suggested two formation mechanisms for the observed intrusions in the Eurasian Basin. (1) Intrusions formed across a wide front in Fram Strait separating the warm and salty inflow and the colder and fresher return flow. (2) Formation across a narrow front at the continental slope north of the Barents Sea where the inflowing Atlantic Water confluences with the cold and fresh water from the Barents Sea. The intrusions are then advected by the mean flow around and across the Eurasian Basin and toward Fram Strait. The presence of double-diffusive processes is considered to be important to maintain the intrusions. *May and Kelley* [2001] discuss the steady state and growth properties of intrusions in the baroclinic front separating the West Spitsbergen Current from the ambient cold and fresh water north of Svalbard.

5.1. Intrusions at Steady State

[48] Although Borneo and ASCOS hydrography demonstrated warm/salty and cold/fresh intrusions, the central Amundsen Basin is a region with small horizontal gradients and is not considered a likely region for formation of such intrusions. Both Borneo and ASCOS had weak background horizontal density gradients, $(0.9 \pm 0.5) \cdot 10^{-7}$ kg m^{-4} and $(-1.0 \pm 0.8) \cdot 10^{-7}$ kg m^{-4}, respectively, between 250–450 m where the intrusions were detected. The change in sign from Borneo to ASCOS reflects a change in sign in both temperature and salinity gradients between the two surveys (Table 4).

[49] Intrusions were detected along the Borneo and ASCOS drifts and by assuming that they were beyond their initial growth phase, the mixing processes involved in maintaining the intrusive structure are investigated, following *May and Kelley* [2001]. From each survey, five profiles were selected such that their positions form a relatively straight line through the survey region. In each profile, three warm/salty intrusions and two cold/fresh intrusions were picked manually. A linear regression of the vertical position of each detected intrusions was used to calculate the slope of the intrusion as

$$s = \left.\frac{\partial z}{\partial x}\right|_l \tag{10}$$

where the vertical position, z, is relative to horizontal geopotential surfaces and l indicates that the gradient is

Table 4. Horizontal and Vertical Background Gradients of Temperature, Salinity and Density for the Lomonosov Ridge Profiles

Background Gradient	Temperature (°C m^{-1})	Salinity (psu m^{-1})	Density (kg m^{-4})
Cross front	-6.7×10^{-6}	-2.4×10^{-7}	3.2×10^{-7}
Vertical	1.1×10^{-3}	-3.1×10^{-4}	-5.0×10^{-3}

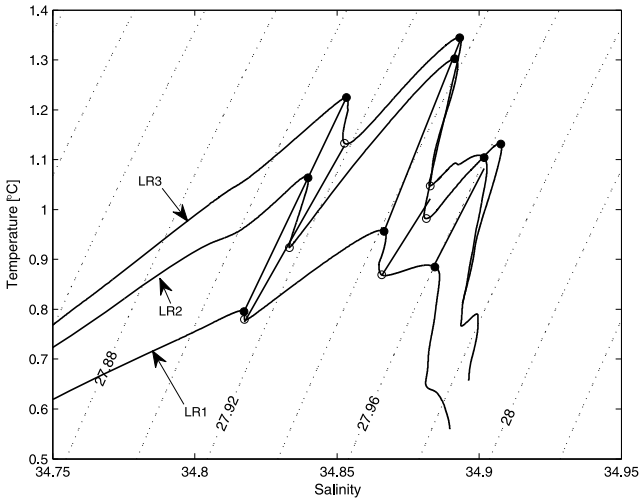

Figure 10. Temperature and salinity diagram for the three Lomonosov Ridge profiles. Circles indicate detected intrusions, where filled circles are warm and salty intrusions and open circles are cold and fresh intrusions. Straight lines are linear regressions of positions of the detected intrusions.

calculated in the direction of the intrusive layer. The slope indicates whether the intrusions slope upward ($s > 0$) or downward ($s < 0$) relative to the horizontal surfaces. The along-intrusion density ratio

$$R_l = \frac{\alpha}{\beta}\frac{\partial T}{\partial S}\bigg|_l \tag{11}$$

was calculated from a linear regression for each intrusion on a *TS* diagram. R_l indicates whether the intrusions slope along the isopycnals ($R_l = 1$) or downward ($R_l > 1$) or upward ($R_l < 1$) relative to the isopycnals, respectively.

[50] Intrusion slopes were $s = (1.2 \pm 0.3) \cdot 10^{-4}$ and $s = (-1.8 \pm 0.5) \cdot 10^{-4}$ for Borneo and ASCOS, respectively, i.e., upward for Borneo and downward for ASCOS, relative to horizontal surfaces. However, R_l was larger than unity for both surveys (Borneo: $R_l = 1.20 \pm 0.03$; ASCOS: $R_l = 1.28 \pm 0.02$) showing that the intrusions in both cases were sloping downward relative to the isopycnals. Intrusions sloping downward relative to isopycnals indicate that diffusive convection is more dominant than salt fingering [*May and Kelley*, 2001].

[51] Both salt fingering and diffusive convection modify the intrusions and for a warm and salty intrusion, both processes lead to a density flux out of the intrusion. In steady state, this loss of density is balanced by advection of a horizontal gradient and balancing these three fluxes provides a ratio of the contribution of diffusive convection relative to salt fingering [*May and Kelley*, 2001]:

$$-\frac{\beta F_S^d - \alpha F_T^d}{\beta F_S^f - \alpha F_T^f} = \frac{\left(R_l - \gamma_f\right)\left(1/\gamma_d - 1\right)}{\left(1 - \gamma_f\right)\left({}^1\!/_{\gamma_d} - R_l\right)} \tag{12}$$

where F_s and F_T is double-diffusive fluxes of salt and heat, respectively and superscript d and f indicate diffusive convection and salt fingering. $\gamma_f \approx 0.6$ is the nondimensional flux ratio for salt fingering [*McDougall and Ruddick*, 1992], and $\gamma_d \approx 0.15$ is the nondimensional flux ratio for diffusive convection [*Kelley*, 1990]. Substituting values for R_l, γ_f and γ_d into (12), yields ratios of 1.6 and 1.8 for Borneo and ASCOS, respectively, which shows that diffusive convection contributes 60% and 80% more than salt fingering in maintaining the steady state intrusions in the central Amundsen Basin. By assuming that the observed intrusions north of Svalbard had reached steady state, *May and Kelley* [2001] found that density fluxes induced by diffusive convection were three times larger than those from salt fingering.

5.2. Cross-Frontal Intrusions at the Lomonosov Ridge

[52] The three stations across the Lomonosov Ridge (LR1–3, Figure 1) contrast the weak horizontal gradient regime at the Borneo and ASCOS surveys. The Lomonosov Ridge is a shear zone with counter flowing currents on each side with significant cross-ridge gradients in temperature and salinity [e.g., *Rudels et al.*, 1999].

[53] Average horizontal and vertical gradients in the depth range of observed intrusions (250–450 m) are tabulated in Table 4. The horizontal gradients in temperature and salinity across the ridge between LR1 and LR3 were larger than those across the frontal region north of Svalbard [*May and Kelley*, 2001]. Temperature and salinity gradients did not fully compensate, hence the front was considered baroclinic with a positive density gradient toward the Makarov Basin side of the ridge (Table 4).

[54] Following the procedure described in section 5.1, we detected the intrusions in LR1–LR3 and estimated s and R_l. The intrusions slope upward toward the cold and fresh side of the front (Figure 11) with $s = (7.0 \pm 4.0) \cdot 10^{-4}$, almost one order of magnitude steeper than in Borneo and ASCOS. Relative to the isopycnals, intrusions slope marginally downward, $R_l = 1.07 \pm 0.03$ (Figure 10).

[55] In the growth stage, both double-diffusive processes can be active in developing the intrusion. By applying predictions from the instability theory for a baroclinic front, *May and Kelley* [2001] developed a set of criteria for s and

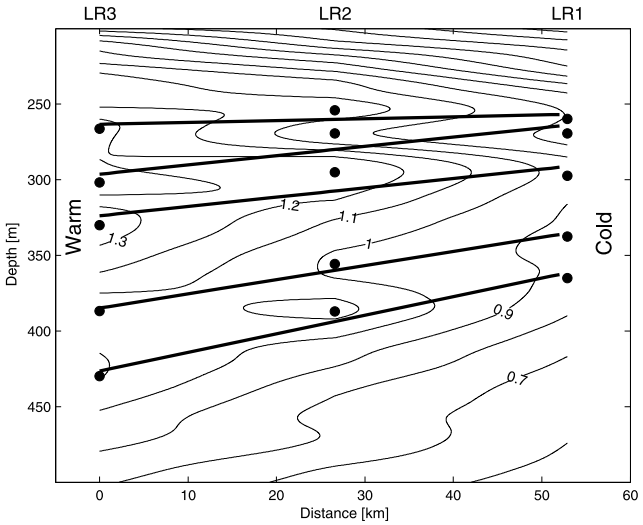

Figure 11. Vertical position of intrusions as function of distance from LR1. Straight lines are linear regressions of vertical position. Contours are isotherms.

R_l to determine which process dominates during growth. Salt fingering dominates when [*May and Kelley*, 1997, 2001]

$$0 < s < -\frac{\left(\alpha\bar{T}_x - \gamma_f\beta\bar{S}_x\right)}{\left(\alpha\bar{T}_z - \gamma_f\beta\bar{S}_z\right)} \qquad \gamma_f < R_l < \frac{\alpha\bar{T}_x}{\beta\bar{S}_x} \tag{13}$$

where subscript x and z denotes horizontal and vertical gradients, respectively and overbars indicate section average gradients. Diffusive convection dominates when:

$$-\frac{(\gamma_d\alpha\bar{T}_x - \beta\bar{S}_x)}{(\gamma_d\alpha\bar{T}_z - \beta\bar{S}_z)} < s < 0 \qquad \frac{\alpha\bar{T}_x}{\beta\bar{S}_x} < R_l < \frac{1}{\gamma_d} \tag{14}$$

[56] Using the observed cross-front and vertical gradients (Table 4), $\gamma_f = 0.6$ and $\gamma_d = 0.15$ yields $0 < s < 1.7 \cdot 10^{-3}$ and $0.6 < R_l < 2.6$ for salt fingering and $-4.6 \cdot 10^{-4} < s < 0$ and $2.6 < R_l < 6.7$ for diffusive convection. The estimated $s = (7.0 \pm 4.0) \cdot 10^{-4}$ and $R_l = 1.07 \pm 0.03$ for LR3–LR1 indicate that salt fingering was the dominant double-diffusive process during the growth stage of the intrusions.

[57] The slope of the intrusions was between the horizontal and the slope of the isopycnals. In a baroclinic front, intrusions with slopes in this range might be reinforced by the baroclinicity, which contributes to the growth of the intrusions [*May and Kelley*, 2001]. Assuming that a density perturbation in an intrusive layer was caused by either salt fingering or advection (due to baroclinicity) [*May and Kelley*, 2001], and using the along-intrusion density ratio and the flux ratio for salt fingering, we find the relative contribution of salt fingering to be four times larger than the contribution from advection of the horizontal density gradient.

6. Summary

[58] Microstructure profiles collected in the central Amundsen Basin were analyzed with emphasis to the role of double-diffusive mixing in vertical heat transfer. More than 500 profiles were collected during two drifts in April and August, 2008. A persistent thermohaline staircase was observed between 200–260 m depth with properties similar to the staircase in the Canada Basin [e.g., *Neshyba et al.*, 1971; *Padman and Dillon*, 1987; *Timmermans et al.*, 2008]. The vertical structure was characterized by an average density ratio $R_\rho \sim 3$ and homogenous layers with an average layer height of 1.3 m separated by thin interfaces with average temperature and salinity jumps of about 0.065°C and 0.015, respectively. The lateral coherence was not resolved.

[59] The average vertical heat flux by diffusive convection through the staircase was estimated to 0.6 W m^{-2}, using the parameterization of *Kelley* [1990]. Heat fluxes were 2 to 3 times larger than those in the Canada Basin, and an order of magnitude smaller than those in the shelf/slope areas of the Arctic Ocean. A thorough examination of the measured turbulent heat fluxes within the high gradient interfaces shows that these fluxes are an order of magnitude smaller and that observations deviate from a "4/3 flux law," especially for a weak thermal forcing (small temperature jump at the interface). This relation fails, perhaps partly because our measurements were unable to resolve the smallest fluxes, but possibly also because the parameterization fails to capture the processes in an oceanographic staircase for weak thermal forcing. An examination of the scaling of the parameterized diffusive convective fluxes shows that the scaling is overestimated by up to an order of magnitude for $R_\rho < 3.5$, but is within a factor of two for $R_\rho > 3.5$. Similarly, the layer height tend to be overestimated by the parameterization for low R_ρ, but agrees well for $R_\rho > 3.5$. Double diffusive staircases are found around warm/salty or cold/fresh intrusions, often observed in the vertical stratification within the Arctic Ocean. Intrusions are suggested to develop from either wide (basin scale) or narrow (e.g., across West Spitsbergen Current) ocean fronts [*Rudels et al.*, 1999]. Analytic considerations also suggest that thermohaline intrusions can develop into staircases for appropriate background density ratios and turbulent mixing [*Merryfield*, 2000]. By examining the baroclinic front across the Lomonosov Ridge, this area is identified as a possible formation region for the observed intrusions and hence important for forming and maintaining the observed vertical segments susceptible for double diffusive processes. An analysis of cross frontal slopes, gradients and density ratios indicates that salt fingering is the most important process in forming the intrusions, whereas diffusive convection contributes significantly more in maintaining them in the central Amundsen Basin.

[60] The most efficient heat loss from the warm Atlantic layer of the Arctic Ocean occurs over shelves and within the boundary currents. Away from topography and boundaries, however, the Arctic water column is quiescent and vertical mixing is limited. Based on parameterizations from laboratory studies, heat transfer by diffusive convection is up to an order of magnitude more efficient than molecular diffusion and the relative importance of diffusive convection can be discussed in light of the overall heat loss from the Atlantic layer of the Arctic Ocean. *Aagaard and Greisman* [1975] estimated the net heat supply to the Arctic within the Atlantic layer of the West Spitsbergen Current to be 55 TW, of which 14 TW is lost to ice melting and exchange with the atmosphere immediately north of Svalbard [*Rudels et al.*, 2008]. Another 12 TW is lost over "hot spots," over ridges, shelves and rough topography assuming that the topographic features cover ~30% of the surface area of the Arctic Ocean [*Fer et al.*, 2010]. The remaining heat, distributed over the abyssal plains, results in an average heat loss from the Atlantic layer of ~4 W m^{-2}. Provided the crude calculations above, the parameterization based heat flux from diffusive convection is significant for the observed cooling of the Atlantic layer in the deep basins. In contrast to hot spots of mixing over rough topography, staircases cover extensive lateral areas of the Arctic basins; albeit the fluxes are small, the contribution to the heat budgets cannot be ignored. But as this study has shown; applying laboratory based parameterizations in the ocean, is not trivial. Understanding the nature of oceanic thermohaline staircases and the possible role of Arctic frontal regions in triggering

thermohaline intrusions and subsequent staircases, merits future research.

[61] **Acknowledgment.** The Borneo field work was funded by the Research Council of Norway through the NORKLIMA Young Investigator grant for IF (178641/S30). The ASCOS (the Arctic Summer Cloud Ocean Study) field work was funded by the Knut and Alice Wallenberg Foundation and DAMOCLES (EU 6th Framework Program). The Swedish Polar Research Secretariat provided access to the icebreaker Oden and logistical support. We are grateful to the Chief Scientists Caroline Leck and Michael Tjernström, and to Oden's Captain Mattias Peterson and his crew. This is publication A400 from the Bjerknes Centre for Climate Research.

References

Aagaard, K., and P. Greisman (1975), Towards new mass and heat budgets for the Arctic Ocean, *J. Geophys. Res.*, *80*(27), 3821–3827, doi:10.1029/JC080i027p03821.

Denman, K. L., and A. E. Gargett (1988), Multiple thermoclines are barriers to vertical exchange in the subarctic Pacific during SUPER, May 1984, *J. Mar. Res.*, *46*(1), 77–103, doi:10.1357/002224088785113739.

Dillon, T. M., and D. R. Caldwell (1980), The Batchelor spectrum and dissipation in the upper ocean, *J. Geophys. Res.*, *85*(C4), 1910–1916, doi:10.1029/JC085iC04p01910.

Dmitrenko, I. A., I. V. Polyakov, S. A. Kirillov, L. A. Timokhov, I. E. Frolov, V. T. Sokolov, H. L. Simmons, V. V. Ivanov, and D. Walsh (2008), Toward a warmer Arctic Ocean: Spreading of the early 21st century Atlantic Water warm anomaly along the Eurasian Basin margins, *J. Geophys. Res.*, *113*, C05023, doi:10.1029/2007JC004158.

Emery, W. J., and R. E. Thomson (2001), *Data Analysis Methods in Physical Oceanography*, vol. XVI, 2nd ed., 638 pp., Elsevier, Amsterdam.

Fer, I. (2006), Scaling turbulent dissipation in an Arctic fjord, *Deep Sea Res., Part II*, *53*(1–2), 77–95, doi:10.1016/j.dsr2.2006.01.003.

Fer, I. (2009), Weak vertical diffusion allows maintenance of cold halocline in the central Arctic, *Atmos. Oceanic Sci. Lett.*, *2*(3), 148–152.

Fer, I., R. Skogseth, and F. Geyer (2010), Internal waves and mixing in the marginal ice zone near the Yermak Plateau, *J. Phys. Oceanogr.*, *40*(7), 1613–1630, doi:10.1175/2010JPO4371.1.

Foldvik, A., and B. Rudels (1996), Double-diffusive experiments, in *Waves and Nonlinear Processes in Hydrodynamics*, edited by J. Grue et al., pp. 239–254, Kluwer Acad., Dordrecht, Netherlands, doi:10.1007/978-94-009-0253-4_19.

Gregg, M. C. (1999), Uncertainties and limitations in measuring ε and χ_T, *J. Atmos. Oceanic Technol.*, *16*(11), 1483–1490, doi:10.1175/1520-0426(1999)016<1483:UALIMA>2.0.CO;2.

Gregg, M. C., and T. B. Meagher (1980), The dynamic response of glass rod thermistors, *J. Geophys. Res.*, *85*(C5), 2779–2786, doi:10.1029/JC085iC05p02779.

Gregg, M. C., and T. B. Sanford (1987), Shear and turbulence in thermohaline staircases, *Deep Sea Res., Part A*, *34*(10), 1689–1696, doi:10.1016/0198-0149(87)90017-3.

Kelley, D. (1984), Effective diffusivities within oceanic thermohaline staircases, *J. Geophys. Res.*, *89*(C6), 10,484–10,488, doi:10.1029/JC089iC06p10484.

Kelley, D. E. (1990), Fluxes through diffusive staircases: A new formulation, *J. Geophys. Res.*, *95*(C3), 3365–3371, doi:10.1029/JC095iC03p03365.

Kelley, D. E., H. J. S. Fernando, A. E. Gargett, J. Tanny, and E. Ozsoy (2003), The diffusive regime of double-diffusive convection, *Prog. Oceanogr.*, *56*(3–4), 461–481, doi:10.1016/S0079-6611(03)00026-0.

Krishfield, R. A., and D. K. Perovich (2005), Spatial and temporal variability of oceanic heat flux to the Arctic ice pack, *J. Geophys. Res.*, *110*, C07021, doi:10.1029/2004JC002293.

Kunze, E. (1994), A proposed flux constraint for salt fingers in shear, *J. Mar. Res.*, *52*(6), 999–1016, doi:10.1357/0022240943076867.

Larson, N. G., and M. C. Gregg (1983), Turbulent dissipation and shear in thermohaline intrusions, *Nature*, *306*(5938), 26–32, doi:10.1038/306026a0.

Lenn, Y. D., et al. (2009), Vertical mixing at intermediate depths in the Arctic boundary current, *Geophys. Res. Lett.*, *36*, L05601, doi:10.1029/2008GL036792.

Marmorino, G. O., and D. R. Caldwell (1976), Heat and salt transport through a diffusive thermohaline interface, *Deep Sea Res.*, *23*(1), 59–67, doi:10.1016/0011-7471(76)90808-1.

May, B. D., and D. E. Kelley (1997), Effect of baroclinicity on double-diffusive interleaving, *J. Phys. Oceanogr.*, *27*(9), 1997–2008, doi:10.1175/1520-0485(1997)027<1997:EOBODD>2.0.CO;2.

May, B. D., and D. E. Kelley (2001), Growth and steady state stages of thermohaline intrusions in the Arctic Ocean, *J. Geophys. Res.*, *106*(C8), 16,783–16,794, doi:10.1029/2000JC000605.

McDougall, T. J., and B. R. Ruddick (1992), The use of ocean microstructure to quantify both turbulent mixing and salt-fingering, *Deep Sea Res., Part A*, *39*(11–12), 1931–1952, doi:10.1016/0198-0149(92)90006-f.

McLaughlin, F. A., E. C. Carmack, W. J. Williams, S. Zimmermann, K. Shimada, and M. Itoh (2009), Joint effects of boundary currents and thermohaline intrusions on the warming of Atlantic water in the Canada Basin, 1993–2007, *J. Geophys. Res.*, *114*, C00A12, doi:10.1029/2008JC005001.

McPhee, M. G., C. Kottmeier, and J. H. Morison (1999), Ocean heat flux in the central Weddell Sea during winter, *J. Phys. Oceanogr.*, *29*(6), 1166–1179, doi:10.1175/1520-0485(1999)029<1166:OHFITC>2.0.CO;2.

Melling, H., R. A. Lake, D. R. Topham, and D. B. Fissel (1984), Oceanic thermal structure in the western Canadian Arctic, *Cont. Shelf Res.*, *3*(3), 233–258, doi:10.1016/0278-4343(84)90010-4.

Merryfield, W. J. (2000), Origin of thermohaline staircases, *J. Phys. Oceanogr.*, *30*(5), 1046–1068, doi:10.1175/1520-0485(2000)030<1046:OOTS>2.0.CO;2.

Mudge, T. D., and R. G. Lueck (1994), Digital signal-processing to enhance oceanographic observations, *J. Atmos. Oceanic Technol.*, *11*(3), 825–836, doi:10.1175/1520-0426(1994)011<0825:DSPTEO>2.0.CO;2.

Muench, R. D., H. J. S. Fernando, and G. R. Stegen (1990), Temperature and salinity staircases in the northwestern Weddell Sea, *J. Phys. Oceanogr.*, *20*(2), 295–306, doi:10.1175/1520-0485(1990)020<0295:TASSIT>2.0.CO;2.

Neshyba, S., V. T. Neal, and W. Denner (1971), Temperature and conductivity measurements under ice island T-3, *J. Geophys. Res.*, *76*(33), 8107–8120, doi:10.1029/JC076i033p08107.

Oakey, N. S. (1982), Determination of the rate of dissipation of turbulent energy from simultaneous temperature and velocity shear microstructure measurements, *J. Phys. Oceanogr.*, *12*(3), 256–271, doi:10.1175/1520-0485(1982)012<0256:DOTROD>2.0.CO;2.

Osborn, T. R. (1980), Estimates of the local rate of vertical diffusion from dissipation measurements, *J. Phys. Oceanogr.*, *10*(1), 83–89, doi:10.1175/1520-0485(1980)010<0083:EOTLRO>2.0.CO;2.

Osborn, T. R., and C. S. Cox (1972), Oceanic fine structure, *Geophys. Fluid Dyn.*, *3*, 321–345, doi:10.1080/03091927208236085.

Padman, L. (1995), Small-scale physical processes in the Arctic Ocean, in *Arctic Oceanography: Marginal Ice Zones and Continental Shelves*, *Coastal Estuarine Stud.*, vol. 49, edited by W. O. Smith and J. Grebmeier, pp. 97–129, AGU, Washington, D.C., doi:10.1029/CE049p0097.

Padman, L., and T. M. Dillon (1987), Vertical heat fluxes through the Beaufort Sea thermohaline staircase, *J. Geophys. Res.*, *92*(C10), 10,799–10,806, doi:10.1029/JC092iC10p10799.

Padman, L., and T. M. Dillon (1988), On the horizontal extent of the Canada Basin thermohaline steps, *J. Phys. Oceanogr.*, *18*(10), 1458–1462, doi:10.1175/1520-0485(1988)018<1458:OTHEOT>2.0.CO;2.

Perkin, R. G., and E. L. Lewis (1984), Mixing in the West Spitsbergen Current, *J. Phys. Oceanogr.*, *14*(8), 1315–1325, doi:10.1175/1520-0485(1984)014<1315:MITWSC>2.0.CO;2.

Polyakov, I. V., A. Pnyushkov, R. Rember, V. V. Ivanov, Y. D. Lenn, L. Padman, and E. C. Carmack (2011), Mooring-based observations of double-diffusive staircases over the Laptev Sea slope, *J. Phys. Oceanogr.*, *42*, 95–109, doi:10.1175/2011jpo4606.1.

Rainville, L., and P. Winsor (2008), Mixing across the Arctic ocean: Microstructure observations during the Beringia 2005 expedition, *Geophys. Res. Lett.*, *35*, L08606, doi:10.1029/2008GL033532.

Robertson, R., L. Padman, and M. D. Levine (1995), Fine-structure, microstructure and vertical mixing processes in the upper ocean in the Western Weddell Sea, *J. Geophys. Res.*, *100*(C9), 18,517–18,535, doi:10.1029/95JC01742.

Ruddick, B. R., and J. S. Turner (1979), Vertical length scale of double-diffusive intrusions, *Deep Sea Res., Part A*, *26*(8), 903–913, doi:10.1016/0198-0149(79)90104-3.

Ruddick, B., D. Walsh, and N. Oakey (1997), Variations in apparent mixing efficiency in the North Atlantic central water, *J. Phys. Oceanogr.*, *27*(12), 2589–2605, doi:10.1175/1520-0485(1997)027<2589:VIAMEI>2.0.CO;2.

Rudels, B., G. Bjork, R. D. Muench, and U. Schauer (1999), Double-diffusive layering in the Eurasian basin of the Arctic Ocean, *J. Mar. Syst.*, *21*(1–4), 3–27, doi:10.1016/S0924-7963(99)00003-2.

Rudels, B., M. Marnela, and P. Eriksson (2008), Constraints on estimating mass, heat and freshwater transports in the Arctic Ocean: An exercise, in *Arctic-Subarctic Ocean Fluxes: Defining the Role of the Northern Seas in Climate*, edited by R. R. Dickson et al., pp. 315–341, Springer, Dordrecht, Netherlands.

Schmitt, R. W. (1994), Double diffusion in oceanography, *Annu. Rev. Fluid Mech.*, *26*, 255–285, doi:10.1146/annurev.fl.26.010194.001351.

Schmitt, R. W., H. Perkins, J. D. Boyd, and M. C. Stalcup (1987), C-SALT: An investigation of the thermohaline staircase in the western tropical North Atlantic, *Deep Sea Res., Part A*, *34*(10), 1655–1665, doi:10.1016/0198-0149(87)90014-8.

Sirevaag, A., and I. Fer (2009), Early spring oceanic heat fluxes and mixing observed from drift stations north of Svalbard, *J. Phys. Oceanogr.*, *39* (12), 3049–3069, doi:10.1175/2009JPO4172.1.

Sirevaag, A., M. G. McPhee, J. H. Morison, W. J. Shaw, and T. P. Stanton (2010), Wintertime mixed layer measurements at Maud Rise, Weddell Sea, *J. Geophys. Res.*, *115*(C2), C02009, doi:10.1029/2008JC005141.

Sirevaag, A., S. de la Rosa, I. Fer, M. Nicolaus, M. Tjernström, and M. G. McPhee (2011), Mixing, heat fluxes and heat content evolution of the Arctic Ocean mixed layer, *Ocean Sci.*, *7*(3), 335–349, doi:10.5194/os-7-335-2011.

Sundfjord, A., I. Fer, Y. Kasajima, and H. Svendsen (2007), Observations of turbulent mixing and hydrography in the marginal ice zone of the Barents Sea, *J. Geophys. Res.*, *112*, C05008, doi:10.1029/2006JC003524.

Thorpe, S. A. (2005), *The Turbulent Ocean*, 439 pp., Cambridge Univ. Press, Cambridge, U. K.

Timmermans, M. L., J. Toole, R. Krishfield, and P. Winsor (2008), Ice-Tethered Profiler observations of the double-diffusive staircase in the Canada Basin thermocline, *J. Geophys. Res.*, *113*, C00A02, doi:10.1029/2008JC004829.

Turner, J. S. (1965), The coupled turbulent transports of salt and and heat across a sharp density interface, *Int. J. Heat Mass Transfer*, *8*(5), 759–767, doi:10.1016/0017-9310(65)90022-0.

Turner, J. S. (2010), The melting of ice in the Arctic Ocean: The influence of double-diffusive transport of heat from below, *J. Phys. Oceanogr.*, *40* (1), 249–256, doi:10.1175/2009JPO4279.1.

You, Y. (2002), A global ocean climatological atlas of the Turner angle: Implications for double-diffusion and water-mass structure, *Deep Sea Res., Part I*, *49*(11), 2075–2093, doi:10.1016/S0967-0637(02)00099-7.